

Magnetic and magnetotransport properties in the Ni-doped $\text{La}_{0.7}\text{Sr}_{0.3}\text{MnO}_3$ system

Ji-Wen Feng

*Institute of Atomic and Molecular Sciences, Academia Sinica, Taipei, Taiwan
and Wuhan Institute of Physics and Mathematics, The Chinese Academy of Sciences, Wuhan 430 071,
People's Republic of China*

C. Ye

*Wuhan Institute of Physics and Mathematics, The Chinese Academy of Sciences, Wuhan 430 071,
People's Republic of China*

Lian-Pin Hwang*

*Department of Chemistry, National Taiwan University, P.O. Box 23-34, Taipei, Taiwan
and Institute of Atomic and Molecular Sciences, Academia Sinica, Taipei, Taiwan*

(Received 17 May 1999; revised manuscript received 1 February 2000)

The magnetic and magnetotransport properties of $\text{La}_{0.7}\text{Sr}_{0.3}\text{Mn}_{1-x}\text{Ni}_x\text{O}_3$ ($x \leq 0.4$) system have been studied. It is found that Ni doping induces a ferromagnetic state to ferromagnetic cluster state transition near the metallic critical threshold composition. Interestingly, the largest low-temperature magnetoresistance (MR) at 77 K is found in the samples in the vicinity of the ferromagnetic threshold composition below which the sample shows both a rapid low-field MR and a slow high-field MR increase and above which only a slow MR increase is observed. The results suggest that the spin-dependent scattering from internal grain regions is also responsible for the low-temperature MR. The low-temperature and low-field MR effect is explained in terms of orientation of the magnetic domains or/and cluster moments associated with the magnetically disordered regions inside grains which may serve as the spin-dependent scattering centers as well as the pinning centers for magnetic domain walls.

I. INTRODUCTION

The hole-doped manganese materials with perovskite structure exhibit a negative colossal magnetoresistance (CMR) effect at the temperature close to T_C ,^{1,2} where they undergo a ferromagnetic-paramagnetic phase transition, accompanied by a metal-insulator transition. A resistivity peak and a CMR peak in most cases are found in the vicinity of the ferromagnetic transition temperature T_C . This intrinsic CMR effect has been explained by the double exchange (DE)^{3,4} interaction between Mn^{4+} and Mn^{3+} ions, which mediates the simultaneous ferromagnetism and metallic conduction. Unfortunately, the CMR effect is usually achieved only in a strong magnetic field in the tesla range, which limits its practical applications.

On the other hand, the macroscopic magnetic and electric properties of real materials can be dramatically modified by various inhomogeneities existed in materials,⁵⁻⁷ such as chemical inhomogeneity, lattice constant, and possible structure inhomogeneities, etc. Among the various inhomogeneities, the effect of grain boundaries discovered recently in the metallic polycrystalline perovskites⁸⁻¹⁴ is of particular interest. Besides the intrinsic CMR peak near T_C , a large low-field magnetoresistance (MR) effect has also been observed over a wide temperature range below T_C , which is absent in single crystals. Different from the intrinsic double-exchange-type CMR, the low-temperature and low-field MR effect is supposed to be from an extrinsic factor—grain boundaries where structural disorder and magnetic disorder do exist. The role of grain boundaries in low-field MR has further been determined by investigating the effects of particle size⁹⁻¹¹

and single grain boundary on epitaxial manganese films.^{15,16} So far, the low-field and low-temperature MR effect has been explained mainly in terms of spin-dependent tunneling across the grain boundaries^{9,10} or spin-dependent magnetic domain scattering at the boundary regions.^{12,14} However, all the observed results above polycrystalline samples do not give any convincing evidence for supporting either spin-dependent tunneling or spin-dependent scattering. In classical sense, if spin-dependent scattering at grain boundaries is responsible for the low-field MR, one may expect that spin-dependent scattering from the intragrain can also cause the low-field MR when such spin-dependent scattering centers exist inside the grains. One approach is to introduce some local spin disorder into the intragrain. This can be done by the direct replacement of Mn by Ni.

In this paper, the magnetism and the related MR behaviors in a series of $\text{La}_{0.7}\text{Sr}_{0.3}\text{Mn}_{1-x}\text{Ni}_x\text{O}_3$ ($x \leq 0.4$) polycrystalline samples have been reported. It is found that the direct replacement of Mn by Ni destroys the long-range ferromagnetic order and induces a ferromagnetic metallic state to cluster-glass-like insulating state transition. Also, Ni doping remarkably influences the low-temperature MR. A largely enhanced low-temperature MR effect is observed in the vicinity of ferromagnetic critical threshold. Furthermore, in order to understand the origins of low-temperature MR effect, the magnetotransport properties of Ni-doped and undoped samples have been compared. The results suggest that the spin-dependent scattering from the internal grain regions is responsible for the large low-field MR in these high-Ni-doped samples rather than the spin-dependent transport across grain boundaries.

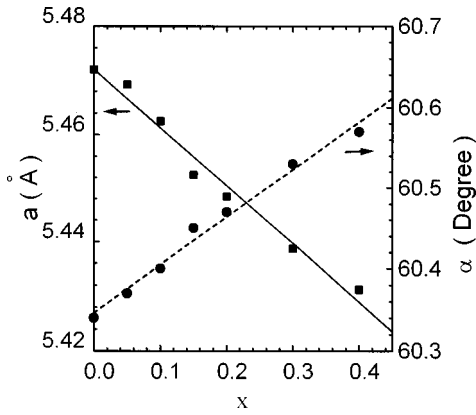


FIG. 1. Lattice parameters for $\text{La}_{0.7}\text{Sr}_{0.3}\text{Mn}_{1-x}\text{Ni}_x\text{O}_3$ samples.

II. EXPERIMENT

A series of ceramic samples $\text{La}_{0.7}\text{Sr}_{0.3}\text{Mn}_{1-x}\text{Ni}_x\text{O}_3$ ($x = 0, 0.05, 0.1, 0.15, 0.18, 0.2, 0.25, 0.3,$ and 0.4) were synthesized by conventional solid-state reaction method in air. Stoichiometric mixtures of La_2O_3 , SrCO_3 , MnO_2 , and NiO were ground, then fired at 800°C for 24 h. The powders thus obtained, were ground, pelletized, and sintered at 1350°C for 70 h with two intermediate grindings. The structure of the samples was characterized by x-ray diffraction (XRD) using $\text{Cu } K\alpha$ radiation and measured at room temperature. The resistivity of the samples was measured by four-probe method. The magnetic field direction was parallel to the current direction. The dependence of magnetization on temperature was measured by a superconducting quantum interference device magnetometer (Quantum Design).

III. RESULT AND DISCUSSION

A. Structure, magnetic, and electronic properties

The powder x-ray diffraction at room temperature shows that all the samples under investigation are of single-phase rhombohedrally distorted perovskite structure (space group $R\bar{3}c$) without any secondary or impurity phase. Although the crystal symmetry of these samples remains the same, their lattice parameters change systematically and smoothly with Ni doping, as shown in Fig. 1. The crystal axis length a decreases and the rhombohedral angle α increases gradually with increasing nickel concentration. This means that the replacement of Mn by Ni increases the rhombohedral distortion. The uniaxial strain $\delta (= \varepsilon_{\parallel} - \varepsilon_{\perp})$ induced by this distortion, for example, is estimated about -2.2×10^{-3} for the sample $x = 0.2$, here ε_{\parallel} and ε_{\perp} represent the strains parallel to and perpendicular to the threefold symmetry axis, respectively.

Figure 2 shows the temperature dependence of magnetization obtained in the zero-field-cooled (ZFC) and the field-cooled (FC) processes with an applied magnetic field of 0.05 T for three typical $\text{La}_{0.7}\text{Sr}_{0.3}\text{Mn}_{1-x}\text{Ni}_x\text{O}_3$ samples ($x = 0.1, 0.2,$ and 0.25). The ZFC magnetization curve indicates that the sample with $x \leq 0.2$ undergoes a paramagnetic to ferromagnetic transition. As nickel content x increases, both Curie temperature T_C and magnetization M are systematically lowered, and the ferromagnetic transition becomes broader. Here the macroscopic Curie temperature T_C is defined as the tem-

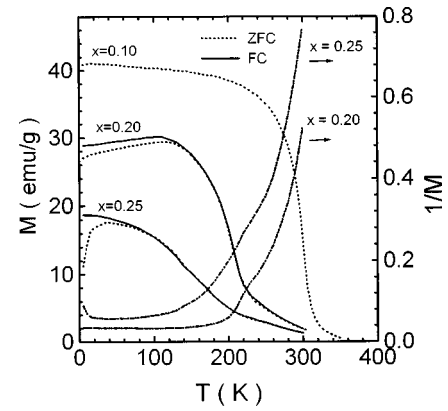


FIG. 2. Left y axis: magnetization as a function of temperature in ZFC and FC processes with applied fields 0.05 T for samples $\text{La}_{0.7}\text{Sr}_{0.3}\text{Mn}_{1-x}\text{Ni}_x\text{O}_3$. Right y axis: reciprocal magnetization $1/M$ as a function of temperature in ZFC process.

perature of the maximum slope in dM/dT . Clearly, the Ni doping suppresses the ferromagnetism. The FC and ZFC data for the sample $x = 0.2$ do not coincide below a relatively high temperature, indicating that some randomly frozen-in magnetic clusters are also present. This illustrates that there is a coexistence of ferromagnetism (possibly the large ferromagnetic regions with multidomain structure) and magnetic clusters for $T < T_C$. Moreover, there is a local maximum around 110 K on both FC and ZFC curves, suggesting the existence of some antiferromagnetic correlation. By contrast, the sample with $x \geq 0.25$ shows the ferromagnetic cluster behaviors without well-defined T_C . Below freezing temperature (T_f), the cluster-glass (or spin-glass) behavior is observed, which is characterized by the difference between the ZFC and FC magnetization data. Moreover, the nonlinearity of reciprocal magnetization $1/M(T)$ can be found far above T_f , suggesting the clustering of magnetic moments. From the above results, it seems that for present $\text{La}_{0.7}\text{Sr}_{0.3}\text{Mn}_{1-x}\text{Ni}_x\text{O}_3$ system there exists a ferromagnetic critical threshold of $x_{cm} \approx 0.2 \sim 0.25$ by crossing which the system evolves into a ferromagnetic cluster state from a ferromagnetic state. The above doping effect on magnetism could be understood in terms of $\text{Mn}^{3+} - \text{Mn}^{4+}$ bond percolation, which will be discussed later.

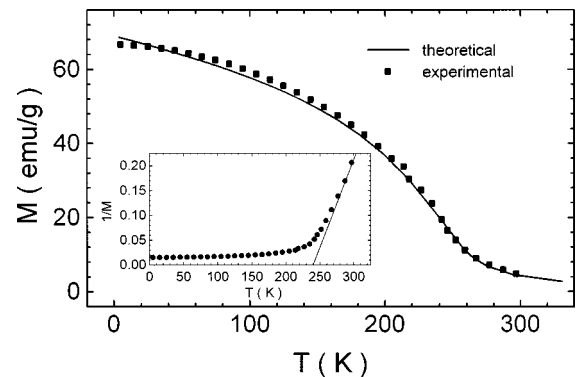


FIG. 3. Temperature dependence of magnetization of $\text{La}_{0.7}\text{Sr}_{0.3}\text{Mn}_{0.8}\text{Ni}_{0.2}\text{O}_3$ at $H = 2$ T. The points are experimental data, the solid is the calculated result. Inset, the reciprocal magnetization $1/M$ as a function of temperature.

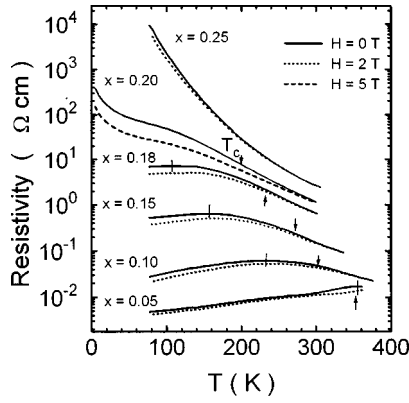


FIG. 4. Temperature dependence of resistivity (at zero field and under an applied field of $H=2$ or 5 T) for $\text{La}_{0.7}\text{Sr}_{0.3}\text{Mn}_{1-x}\text{Ni}_x\text{O}_3$. Arrows and vertical lines indicate the Curie temperature and the metal-insulator transition temperature, respectively.

Figure 3 shows the temperature dependence of magnetization at $H=2$ T for the sample $x=0.2$. To better understand the behavior of $M(T)$, a simple classical mean-field model is used to parameterize the observed data. According to the mean-field model the magnetization is expressed as^{17,18}

$$\frac{M}{M_S} = L(\alpha) \quad (1)$$

with $L(\alpha) = \coth(\alpha) - 1/\alpha$ and

$$\alpha = \frac{\mu H}{k_B T} + \frac{3T_C M}{TM_S}, \quad (2)$$

where k_B is the Boltzmann constant. The above equations contain three independent parameters: M_S , the mean-field saturation moment, T_C , the mean-field Curie temperature, and μ , the magnetic moment of the basic magnetic clusters whose internal degrees of freedom are regarded to be frozen in the energy range of concern. The high-temperature data, as shown in the inset of Fig. 2, are used to estimate the mean-field Curie temperature T_C and the Curie constant $C = \mu M_S / 3k_B$. Taking the value of magnetization (5 K) under 2 T as M_S , $T_C = 240$ K and $\mu = 3k_B C / M_S \approx 7\mu_B$ are thus obtained. By substituting this set of parameters into Eqs. (1) and (2), one can calculate the magnetization curve $M(T)$. The calculated result is also given in Fig. 3. From Fig. 3 it can be seen that the experimental data $M(T)$ are well described by the simple mean-field model. However, it is worth pointing out that the experimental value of magnetization under $H=2$ T at 5 K is still about 12% lower than the theoretical saturation magnetization. This may be attributed to the local disordered or canted spin alignment from the competing ferromagnetic double exchange and antiferromagnetic superexchange. While the effect of magnetic anisotropy (mainly from the magnetostrictive strain and with the order of magnitude 1×10^5 erg/cm³ (Ref. 19) on magnetization due to single frozen clusters is considered to be smaller under a field of 2 T.

Figure 4 shows the temperature dependence of resistivity (ρ) of $\text{La}_{0.7}\text{Sr}_{0.3}\text{Mn}_{1-x}\text{Ni}_x\text{O}_3$ ($x \leq 0.4$) series at several different magnetic fields, where the arrow and vertical line indicate the Curie temperature and the position of the resistiv-

ity peak, respectively. Obviously, the zero-field resistivity increases systematically with Ni doping. For the sample with $x \leq 0.05$, a metal-insulator transition, characterized by a resistivity peak, occurs near the Curie temperature T_C . By contrast, for the sample with $0.1 \leq x < 0.2$, such a resistivity peak appears at a temperature far below T_C , and decreases in temperature with the increasing nickel concentration. The resistivity peak appearing at a temperature much lower than the Curie temperature has also been observed in some other manganese perovskites^{5,6} and ascribed to the inhomogeneities existed in these systems. For the present case, it may be related to the local magnetic disorder arising from statistical composition fluctuations or atomic short-range order due to Ni doping. However, for $x \geq 0.2$ no any resistivity peak can be seen and the sample exhibits the insulating behavior in the whole experimental temperature range, either with or without application of the magnetic field. The above results show that Ni doping induces a metal-insulator transition. The metallic threshold composition is determined as $x_c \approx 0.2$ by the change of resistivity temperature coefficient ($d\rho/dT$) at low temperature range from positive in the metallic regime below the threshold to negative in the insulating regime above it. It is noted that this metallic threshold composition is close, but never exactly equal to the ferromagnetic critical threshold.

Summarizing the above low-temperature electronic phases together with the corresponding magnetic phases, there are three distinct phase regimes in $\text{La}_{0.7}\text{Sr}_{0.3}\text{Mn}_{1-x}\text{Ni}_x\text{O}_3$ ($x \leq 0.4$): (i) ferromagnetic metallic regime for $x \leq 0.18$; (ii) cluster-glass (or spin-glass)-type insulating regime for $x \geq 0.25$, and (iii) transition regime ($x \sim 0.2$) where the low-temperature insulating phase exhibits the supposition of ferromagnetic behavior and magnetic cluster behavior. In previous study of the $\text{La}_{0.8}\text{Sr}_{0.2}\text{Mn}_{1-x}\text{Cu}_x\text{O}_3$, only ferromagnetic metallic phase [regime (i)] and spin-glass-like insulator [regime (ii)] were investigated.⁵

It is well known that the double exchange between Mn^{3+} and Mn^{4+} mediates ferromagnetism and metallic conductance. When Ni is doped into the samples, it occupies randomly the Mn site in the lattice, which no longer effectively participates in the double exchange processes. It seems that in the $\text{La}_{0.7}\text{Sr}_{0.3}\text{Mn}_{1-x}\text{Ni}_x\text{O}_3$ a percolation of the $\text{Mn}^{3+}/\text{Mn}^{4+}$ pairs is necessary to simultaneously install double-exchange-like ferromagnetism and metallic conductance. By taking the probability of $\text{Mn}^{3+}/\text{Mn}^{4+}$ pairs as the metallic critical percolation probability in $\text{La}_{0.83}\text{Sr}_{0.17}\text{MnO}_3$ where low-temperature ferromagnetic metallic phase starts appearing,²⁰ one can get an estimate of the metallic percolation threshold of $x_c \approx 0.23$ for $\text{La}_{0.7}\text{Sr}_{0.3}\text{Mn}_{1-x}\text{Ni}_x\text{O}_3$. This value is in good agreement with the observed ferromagnetic critical threshold ($x_c \approx 0.20$).

In the ferromagnetic metallic regime, there exists a metallic continuum including some magnetically disordered regions centered at Ni ions. Spins in these regions are disordered or canted due to the locally weakened double exchange and the competing superexchange coupling.⁵ In this case, the sample is metallic, and the resistivity increases with Ni doping, owing to the strong electron scattering from magnetically disordered regions. While in the ferromagnetic cluster regime, due to fewer pairs of $\text{Mn}^{3+}/\text{Mn}^{4+}$, only some isolated ferromagnetic clusters can form in the Mn-rich regions, and they are buried in the insulating matrix that is magneti-

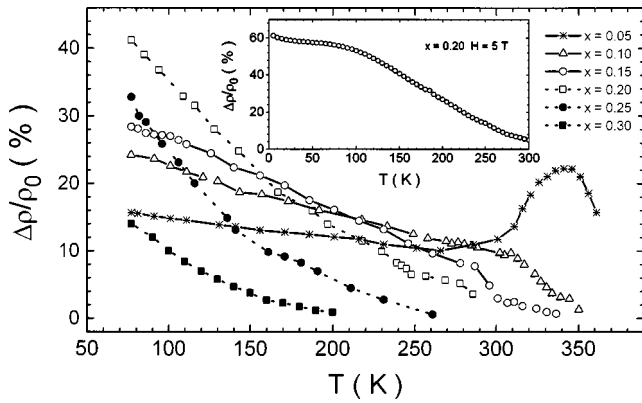


FIG. 5. MR ratio as a function of temperature at 2 T for $\text{La}_{0.7}\text{Sr}_{0.3}\text{Mn}_{1-x}\text{Ni}_x\text{O}_3$. Inset, The MR ratio as a function of temperature at 5 T for the sample with $x=0.20$.

cally disordered. In this case, the conductance of the sample is controlled by electron transport across the insulating regions. Thus as a whole the sample is insulating. As for in the transition regime, the ferromagnetic metallic continuum is broken up into some large ferromagnetic regions and some small magnetic clusters, which leads to the supposition of ferromagnetic behavior and magnetic cluster behavior. The sample in this regime may also behave as an insulator at low temperature due to strong electron scattering from the increasingly magnetic disordered regions.

B. Magnetoresistance

The MR ratio as a function of temperature at $H=2$ T for $\text{La}_{0.7}\text{Sr}_{0.3}\text{Mn}_{1-x}\text{Ni}_x\text{O}_3$ is plotted in Fig. 5. The MR ratio is defined as $\Delta\rho/\rho_0 = (\rho_0 - \rho_H)/\rho_0$, where ρ_0 is the zero-field resistivity and ρ_H is the resistivity in the applied field H . For the sample with $x \leq 0.05$, a MR peak that is close to both Curie temperature and metal-insulator transition temperature can clearly be seen. This may be interpreted as the CMR component related to insulator-metal transition. However, for the sample with $x \geq 0.1$, no MR peak can be observed in the experimental temperature range whether the sample exhibits a metal-insulator transition or not. Furthermore, a significant MR ratio ($H=2$ T) appears in the low-temperature range for all samples, either metallic or insulating, and increases monotonically with decreasing temperature. It is noteworthy that the sample with $x=0.2$ which is near the ferromagnetic critical threshold exhibits a largely enhanced low-temperature MR ratio of about 60% at $H=5$ T (see the inset in Fig. 5) or about 40% at $H=2$ T (77 K). The above results reveal that Ni doping reduces the intrinsic CMR effect and enhances low-temperature MR effect for the sample with $x \leq 0.30$. It is not surprising that Ni doping suppresses the CMR component. The zero-field resistivity ρ_0 is increasingly influenced by the presence of magnetically disordered regions. This together with that the change of resistivity ($\Delta\rho$) induced by applied field near T_C decreases due to the broadening of ferromagnetic transition, gives rise to the reduction in CMR ratio.

It is worth mentioning that the magnetotransport behavior in present $\text{La}_{0.7}\text{Sr}_{0.3}\text{Mn}_{1-x}\text{Ni}_x\text{O}_3$ system at low temperature is somewhat similar to that obtained in heterogeneous ferro-

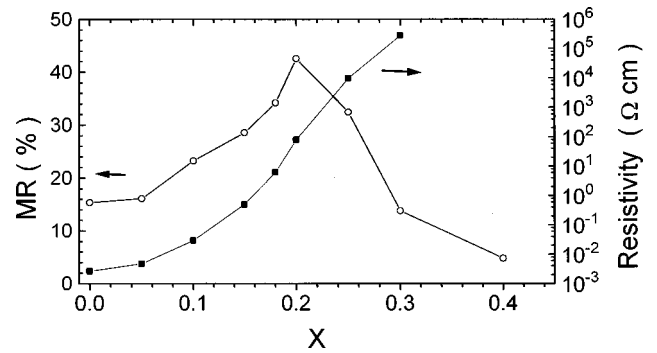


FIG. 6. Zero-field resistivity and MR ratio ($H=2$ T) as functions of nickel content at 77 K for $\text{La}_{0.7}\text{Sr}_{0.3}\text{Mn}_{1-x}\text{Ni}_x\text{O}_3$.

magnetic metal-insulator mixture. For convenience, the zero-field resistivity and MR ratio ($H=2$ T) as a function of nickel content at 77 K are summarized in Fig. 6. Two important features should be noted in the Fig. 6. First, the MR ratio reaches its maximum of about 40% at $x_c \approx 0.2$, which is located in the vicinity of the ferromagnetic critical threshold. Second, the resistivity increases rapidly near and above this threshold composition. The similar phenomena have also been observed in the heterogeneous granular ferromagnetic metal-insulator mixture.²¹

Figure 7 shows the MR ratio as a function of the applied field H at 77 K for the samples $x=0, 0.15, 0.20$, and 0.25 . An important feature in Fig. 7 is that the sample with $x \leq 0.2$, which is ferromagnetic or ferromagnetic+cluster magnetic, exhibits a sharp MR increase at low field H (< 1.2 kOe) (i.e., so-called low-field MR effect) followed by a slow but still significant increase at higher field. The high-field MR increase is more remarkable in the sample with higher nickel content. Here, an important fact which should be emphasized is that the low-field MR ratio does not decrease obviously with increasing Ni doping for the sample with $x \leq 0.20$ even though the low-temperature resistivity increases by several orders of magnitude (also see Fig. 6). However, for the sample with $x=0.25$ that exhibits cluster-like (or spin-glass) magnetism, the low-field MR effect is not obvious, and a large MR ratio can be achieved only at a much higher applied field.

Low-temperature MR has a low-field and high-field component. This has also been observed in some other polycrystalline manganites, and attributed to the different physical

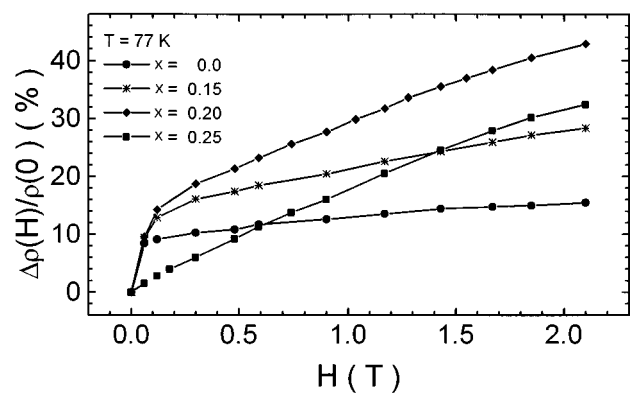


FIG. 7. Variation in $\Delta\rho/\rho_0$ with applied field H at 77 K for $\text{La}_{0.7}\text{Sr}_{0.3}\text{Mn}_{1-x}\text{Ni}_x\text{O}_3$.

origins.^{6,8,9,12,14} The low-temperature but high-field MR behavior has been explained in terms of alignments of the neighboring Mn spins inside the grains or at the grain boundaries.^{6,8,14} Similarly, the high-field MR behavior observed in the present Ni-doped $\text{La}_{0.7}\text{Sr}_{0.3}\text{MnO}_3$ system can also be interpreted in terms of the alignments of Mn spins in the magnetically disordered regions centered around Ni ions. The spins of ions in these regions are disordered or canted, and aligned gradually with increasing magnetic field. Therefore electrons may transfer more easily between Mn^{3+} and Mn^{4+} ions, leading to MR. In this case, application of a large magnetic field is usually needed to align the neighboring spins completely. Moreover, with increasing Ni doping, magnetically disordered regions increase, thus leading to the enhanced high-field MR.

In the previous studies, on the other hand, the low-temperature and low-field MR effect has been explained in terms of spin-polarized electron transport across the grain boundary regions where the structural and magnetic disorders are regarded as tunneling barriers (intergrain spin-polarized tunneling model)^{9,10} or strong scattering centers (spin-polarized scattering model).^{12,14} In both tunneling and scattering models, the magnetotransport depends on the relative magnetization orientations of two neighboring grains. Moreover, both tunneling and scattering models predicate a low-field MR effect. In our case, the resistivity contribution for the undoped sample is mainly from the grain boundaries, and therefore the low-field MR can also be ascribed to the spin-polarized transport across the grain boundary regions. However, the resistivity at 77 K for the sample with $x = 0.15$ or 0.20 is about three or four orders of magnitude higher than that of the undoped sample (also see Fig. 4). Such a large resistivity is expected to be from the intragrain contribution rather than from the intergrain (grain boundaries) due to the strongly spin-disordered scattering inside the grains. The above fact implies that the grain boundary contribution to low-field MR can be neglected and the low-field MR effect is related to the internal regions of grains. A possible cause is suggested for the low-field MR effect observed in the present Ni-doped samples. The magnetically disordered regions (centered around Ni ions) inside grains, introduced by Ni doping, may serve as the pinning centers for magnetic domain walls as well as the strong spin-scattering centers. A moderately low field can reduce the

scattering because of the alignment of the neighboring domains or/and cluster moments associated with these disordered regions. As for the samples with $x \geq 0.25$, only a slow MR increase at 77 K is found in both low-field and high-field ranges. Apparently, the disappeared ferromagnetism (also disappeared magnetic multidomain structure) is responsible for lack of the low-field MR in these samples. A further interpretation can be made by considering the following two points. First, the clusters for the samples with $x \geq 0.25$ are in superparamagnetic state at 77 K. Therefore the moments of clusters cannot be easily aligned by the applied field due to their thermal fluctuation. Second, for the small clusters the MR contribution from the spin alignment of ions at cluster surfaces becomes dominant, which leads to the high-field MR effect.

IV. CONCLUSION

In summary, the magnetic and magnetotransport properties of $\text{La}_{0.7}\text{Sr}_{0.3}\text{Mn}_{1-x}\text{Ni}_x\text{O}_3$ ($x \leq 0.4$) system have been studied. In the low-doping regime, Ni doping suppresses both ferromagnetic transition and metal-insulator transition, and causes a metal-insulator transition to occur at a temperature far below the Curie temperature. The CMR peak is weakened and even becomes unobservable with increasing Ni doping. Moreover, Ni doping induces a metal-to-insulator transition at a critical nickel composition close to which the system evolves into a cluster-glass state from a ferromagnetic state. Interestingly, the largest low-temperature magnetoresistance at 77 K is found in the samples in the vicinity of the metallic continuity threshold below which the sample shows both low- and high-field MR effects and above which the sample exhibits only a high-field MR effect. The results reveal that besides the grain boundaries the spin-dependent scattering from the internal grain regions also plays an important role in both the low-field and high-field MR.

ACKNOWLEDGMENTS

Authors thank IAMS and the National Science Council for the financial support. One of us (J.W.F.) wishes to thank the members of IAMS for their hospitality, and also to thank IAMS for a fellowship.

*Author to whom correspondence should be addressed.

¹R. Von Helmolt, J. Wecker, B. Holzapfel, L. Shulz, and K. Samwer, Phys. Rev. Lett. **71**, 2331 (1993).

²S. Jin, T. H. Tfeel, M. McCormack, R. Ramesh, and L. H. Chen, Science **264**, 413 (1994).

³C. Zener, Phys. Rev. **82**, 403 (1951). P.-G. de Gennes, *ibid.* **118**, 141 (1960).

⁴P. W. Anderson and H. Hasegawa, Phys. Rev. **100**, 675 (1955).

⁵R. von Helmolt, L. Haupt, K. Barner, and U. Sondermann, Solid State Chem. **82**, 693 (1992).

⁶J. R. Sun, G. H. Rao, and Y. Z. Zhang, Appl. Phys. Lett. **72**, 3208 (1998).

⁷Lide M. Rodriguez-Martinez and J. Paul Attfield, Phys. Rev. B **54**, R15 622 (1996).

⁸H. L. Ju, J. Gopalakrishnan, J. L. Peng, Qi Li, G. C. Xiong, T.

Venkatesan, and R. L. Greene, Phys. Rev. B **51**, 6143 (1995).

⁹H. Y. Hwang, S-W. Cheong, N. P. Ong, and B. Batlogg, Phys. Rev. Lett. **77**, 2041 (1996).

¹⁰Ning Zhang, Weiping Ding, Wei Zhong, Dingyu Xing, and Youwei Du, Phys. Rev. B **56**, 8138 (1997).

¹¹R. Mahesh, R. Mahendiran, A. K. Raychaudhuri, and C. N. R. Rao, Appl. Phys. Lett. **68**, 2291 (1996).

¹²X. W. Li, A. Gupta, Gang Xiao, and G. Q. Gong, Appl. Phys. Lett. **71**, 1124 (1997).

¹³P. Schiffer, A. P. Ramirez, W. Bao, and S.-W. Cheong, Phys. Rev. Lett. **75**, 3336 (1995).

¹⁴A. Gupta, G. Q. Gong, Gang Xiao, P. R. Duncombe, P. Lecoeur, P. Trouilloud, Y. Y. Wang, V. P. Dravid, and J. Z. Sun, Phys. Rev. B **54**, R15 629 (1996).

¹⁵N. D. Mathur, G. Burnell, S. P. Isaac, T. J. Jackson, B.-S. Teo, J.

- L. MacManus-Driscoll, L. F. Cohen, J. E. Evetts, and M. G. Blamire, *Nature (London)* **387**, 266 (1997).
- ¹⁶K. Steenbeck, T. Eick, K. Kirsch, K. O'Donnell, and E. Steinbeiß, *Appl. Phys. Lett.* **71**, 968 (1997).
- ¹⁷J. I. Gittleman, Y. Goldstein, and S. Bozowski, *Phys. Rev. B* **5**, 3609 (1972).
- ¹⁸J. Z. Sun, L. Krusin-Elbaum, A. Gupta, Gang Xiao, and S. S. P. Parkin, *Appl. Phys. Lett.* **69**, 1002 (1996).
- ¹⁹J. O'Donnell, M. S. Rzechowski, J. N. Eckstein, and I. Bozovic, *Appl. Phys. Lett.* **72**, 1775 (1998).
- ²⁰A. Urushibara, Y. Moritomo, T. Arima, A. Asamitsu, G. Kido, and Y. Tokura, *Phys. Rev. B* **51**, 14 103 (1995).
- ²¹A. Milner, A. Gerber, B. Groisman, M. Karpovsky, and A. Gladkikh, *Phys. Rev. Lett.* **76**, 475 (1996).